

# EEGDM: Learning EEG Representation with Latent Diffusion Model

Shaocong Wang<sup>†</sup>, Tong Liu<sup>†</sup>, Yihan Li, Ming Li, Kairui Wen, Pei Yang, Wenqi Ji, Minjing Yu, and Yong-Jin Liu<sup>\*</sup>

**Abstract**—Recent advances in self-supervised learning for EEG representation have largely relied on masked reconstruction, where models are trained to recover randomly masked signal segments. While effective at modeling local dependencies, such objectives are inherently limited in capturing the global dynamics and long-range dependencies essential for characterizing neural activity. To address this limitation, we propose EEGDM, a novel self-supervised framework that leverages latent diffusion models to generate EEG signals as an objective. Unlike masked reconstruction, diffusion-based generation progressively denoises signals from noise to realism, compelling the model to capture holistic temporal patterns and cross-channel relationships. Specifically, EEGDM incorporates an EEG encoder that distills raw signals and their channel augmentations into a compact representation, acting as conditional information to guide the diffusion model for generating EEG signals. This design endows EEGDM with a compact latent space, which not only offers ample control over the generative process but also can be leveraged for downstream tasks. Experimental results show that EEGDM (1) reconstructs high-quality EEG signals, (2) learns robust representations, and (3) achieves competitive performance across diverse downstream tasks, thus exploring a new direction for self-supervised EEG representation learning.

**Index Terms**—Self-supervised learning, diffusion model, EEG representation learning.

## I. INTRODUCTION

LECTROENCEPHALOGRAPHY (EEG) is a non-invasive technique that measures spontaneous electrical activity in the brain through scalp electrodes. The interpretation and utilization of EEG signals generally require sophisticated signal processing pipelines and advanced feature extraction methodologies [1]. Conventional EEG signal analysis typically employs manually engineered operations tailored to specific EEG features of interest (e.g., band-pass filtering in a specific frequency range), potentially excluding other informative signal components [2].

Recently, deep learning has introduced a new research paradigm for EEG signal analysis due to its capability to automatically learn efficient representations from original data [3]–[5]. Current deep learning-based approaches, which

This work was supported in part by the National Natural Science Foundation of China (U2336214). (\* Corresponding author: Yong-Jin Liu.)

Shaocong Wang, Tong Liu, Yihan Li, Ming Li, Kairui Wen, Pei Yang, Wenqi Ji and Yong-Jin Liu are with the MOE-Key Laboratory of Pervasive Computing, Department of Computer Science and Technology, Tsinghua University, Beijing 100084, China (e-mail: wangsc23@tsinghua.edu.cn; tongliu@tsinghua.edu.cn; liyihan23@mails.tsinghua.edu.cn; mingli\_thu@tsinghua.edu.cn; wkr21@mails.tsinghua.edu.cn; yangpei20@mails.tsinghua.edu.cn; jwq21@mails.tsinghua.edu.cn; liuyongjin@tsinghua.edu.cn).

Minjing Yu is with the College of Intelligence and Computing, Tianjin University, Tianjin 300350, China (e-mail: minjingyu@tju.edu.cn).

<sup>†</sup> These authors contributed equally.

predominantly rely on large-scale EEG datasets, can be broadly classified into two categories: (1) task-specific models, and (2) multi-task large models. Task-specific models face significant challenges in generalization due to substantial variations across datasets in channel configurations, sampling rates, and EEG recording time lengths. These discrepancies necessitate model training on individual datasets, thereby severely limiting cross-dataset generalizability. For multiple tasks, three large EEG models, EEGPT [6], LaBraM [7], and CBraMod [8] have recently been proposed. These models learn generic representations through masked reconstruction pre-training objective before being fine-tuned for various downstream tasks. However, masked reconstruction has limited capacity in capturing the global dynamics and long-term dependencies essential for characterizing neural activity.

In this paper, we introduce the Diffusion Model (DM) [9], [10] into EEG representation learning and propose a novel self-supervised framework called EEGDM. Our framework leverages EEG signal synthesis as a self-supervised objective, turning the diffusion model into a strong representation learner capable of capturing EEG semantics. Unlike popular masked reconstruction approaches that primarily focus on local feature recovery, DM learns effective representations through a self-supervised denoising objective that requires understanding the underlying data distribution [9]. This makes DM potentially valuable for generic EEG representation learning. Building on this observation, our framework uses an EEG encoder that transforms input signals and their channel augmentations into compact latent representations, which condition the diffusion process. This design enables the encoder to learn the effective and generic representations inherent in EEG signals that are crucial for downstream tasks.

We note that EEG signals present unique challenges due to their inherently low signal-to-noise ratio (SNR) and complex characteristics, including stochasticity, nonstationarity, and non-linearity [11], [12]. To address these challenges, we incorporate two key technical components in our EEGDM framework. First, we employ channel augmentation that provides diverse training perspectives while enriching the conditional information. Second, we utilize Principal Component Analysis (PCA) to project EEG signals into a latent space with an improved SNR, as it enhances signal-relevant components while suppressing noise-related ones [13]. This transformation mitigates the challenge of reconstructing the original noisy signal. Inspired by the success of state-of-the-art DMs (e.g., Latent Diffusion Models (LDMs) [14] and Diffusion Transformers (DiTs) [15]) operating in latent spaces, we apply our DM to this PCA-derived latent space rather than the original noisy EEG

space. This enables EEGDM to focus on learning meaningful signal patterns for effective representation learning across diverse downstream tasks. Our experiments show that EEGDM effectively learns robust representations, achieving competitive performance across diverse downstream tasks and exhibiting strong generalizability.

Our contributions are summarized as follows:

- We propose EEGDM, a novel diffusion model-based self-supervised framework for EEG representation learning. By leveraging EEG signal generation as the self-supervised objective, EEGDM transforms the diffusion model into a powerful representation learner that captures rich EEG semantics.
- EEGDM incorporates channel augmentation and elaborately designed PCA-based latent space operations to (1) enhance the conditional information available for DM, (2) enable robust EEG signal reconstruction, and (3) improve the cross-dataset generalizability of learned EEG representations.
- We validate the effectiveness and generalizability of EEGDM across multiple EEG analysis tasks, demonstrating its (1) competitive performance compared to existing methods and (2) strong cross-dataset transferability and practical utility in EEG applications.

The remainder of this work is organized as follows. First, we describe the related works in Section II. Next, the proposed algorithm is introduced in detail in Section III. After that, experimental results are shown in Section IV. Finally, the conclusion is given in Section V.

## II. RELATED WORK

### A. Self-supervised EEG Representation Learning

Self-supervised learning can leverage large amounts of unlabeled data for pre-training, thereby reducing the reliance on manual annotations. This methodology has led to significant breakthroughs in natural language processing and computer vision [16], [17]. However, its full potential in EEG analysis remains largely unexplored [18].

Some studies [1], [19] have explored learning representations of EEG signals via contrastive learning, which trains a channel feature extractor by extending the SimCLR framework [20] to time series data. Another line of work extends the mask idea to EEG analysis [21]. For instance, Chien et al. [22] propose a masked auto-encoder, which learns the EEG representation by learning to reconstruct the masked EEG features using a Transformer architecture. BENDR [23] uses a convolutional encoder to extract EEG features from local time windows, masks a portion of them, and utilizes a Transformer to predict the information in the masked part. LaBraM [7] pre-trains a Transformer model by predicting the original neural codes of masked EEG channel patches based on a defined neural codebook. EEGPT [6] introduces the alignment of spatio-temporal representation, implemented by a mask-based dual self-supervised learning for efficient extraction of EEG features. CBraMod [8] introduces a structurally aware EEG foundation model that separately captures heterogeneous spatial-temporal dependencies through a criss-cross transformer and achieves

strong cross-dataset generalization via large-scale masked pre-training.

Unlike the above approaches, we explore self-supervised EEG representation learning via generative models. Our proposed EEGDM not only facilitates high-quality EEG generation but also enables the learning of rich and robust representations for downstream tasks.

### B. Diffusion Model

Diffusion models learn complex data distributions through a progressive denoising process that requires a deep understanding of the underlying data structure and semantics. This fundamental characteristic endows them with dual capabilities: generating high-quality samples and learning meaningful representations inherent in the data distribution. The pioneering work by Sohl-Dickstein et al. [24] and subsequent advances by Ho et al. [9] established diffusion models as powerful tools, leading to widespread applications in generative tasks [14], [15], [25]. More recently, their potential for representation learning has gained attention, with emerging studies showing promising results in learning discriminative features [26]–[28].

In the EEG domain, existing diffusion-based approaches have primarily focused on generative applications, such as EEG synthesis and data augmentation [29]–[31], or a few specific supervised tasks [32], [33]. However, the potential of diffusion models for generic EEG representation learning remains largely unexplored. This presents a significant opportunity, as learning the complex temporal and spatial characteristics of EEG signals can benefit from the understanding of rich data distributions inherent in diffusion models' denoising process. In this paper, we present a novel method that exploits the representational capacity of diffusion models for self-supervised EEG representation learning.

## III. METHOD

Our study is motivated by the following observation: Diffusion models capable of generating rich and high-fidelity content from scratch are likely to effectively characterize the underlying properties, structures, and dynamics of the data during the generative process. Therefore, we explore self-supervised EEG representation learning via the diffusion model, and design the following framework architecture.

### A. Framework Architecture

Our proposed self-supervised EEG representation learning framework, EEGDM, is formulated as a latent diffusion model (DM) conditioned on EEG channel augmentation. Our goal is to generate high-quality EEG signals while equipping the model with a generalizable understanding of EEG data that can be effectively adapted to various downstream tasks. It is worth noting that in the denoising process of DM, directly reconstructing raw EEG signals is challenging due to their inherently low SNR. To address this, we utilize PCA to preprocess the original EEG for noise reduction, and perform the reconstruction on the preprocessed EEG data with a relatively high SNR. The overall architecture of EEGDM is illustrated in Fig. 1.

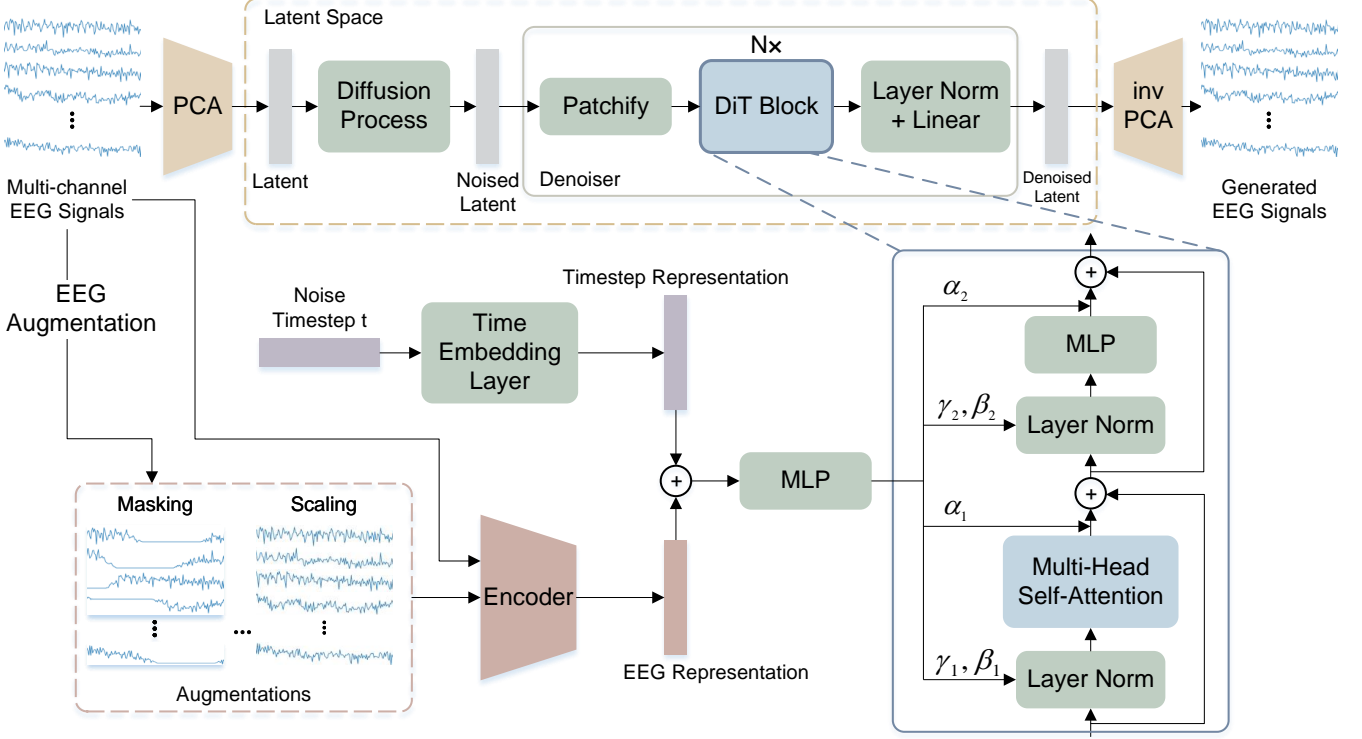


Fig. 1: The overall architecture of EEGDM. The original EEG data is projected onto a latent space using PCA. Noise is added in this latent space, and the denoised latent representation is predicted by learning the conditional latent diffusion model. The prediction is then projected back to the original space by inverse PCA to obtain the generated target EEG signal. The encoder transforms the source EEG signal (including original data and augmentations) into a concise EEG representation. It is combined with the noise timestep representation and then used as conditional information to modulate the DiT block, thus guiding the denoising of the latent representation.

Specifically, given the original multi-channel EEG signals  $X \in \mathbb{R}^{C \times T}$ , where  $C$  is the number of EEG electrodes (channels) and  $T$  is the total timestamp, we segment  $X$  into  $\lfloor \frac{T-t^s}{s^t} \rfloor + 1$  samples. This segmentation assumes a timestamp length<sup>1</sup>  $t^s$  per sample and a stride  $s^t$ . As shown in Fig. 1, each multi-channel sample  $x \in \mathbb{R}^{C \times t^s}$  is processed by PCA to obtain the latent representation  $z$ . Our diffusion model operates on this latent space, where noise is added and predicted. The denoised latent representation predicted by the diffusion model is projected back to the original space by inverse PCA to obtain the target EEG signal. Owing to the effectiveness of the DiT model in the latent space, we utilize it to predict the denoised latent representations. Furthermore, we introduce an EEG encoder that transforms the input source signal  $x'$  (including original EEG sample and its augmentations) into an EEG representation containing rich semantic information. The sum of this EEG representation and the noise timestep representation (i.e., timestep  $t$  in the noise-adding process) encoded by the time embedding layer serves as the conditional input information for the diffusion model. This diffusion model design can utilize the semantically rich external EEG representation for the generative task, leading to a significant

improvement in generative performance. Consequently, this enhances the model's representation learning capability.

### B. The EEG Encoder

The representation output from the EEG encoder lies at the core of EEGDM, which (1) acts as the communication bridge between the encoder and the denoiser ( $\epsilon_\theta$ ), and (2) guides the denoising process. In more details, this output represents a clean source EEG signal semantically related to the target EEG data. The introduction of the encoded EEG representation is to enable hidden states of the diffusion model to predict noise-invariant and semantically meaningful EEG representations from noisy inputs, guiding the reconstruction of the target EEG data during the denoising process.

The core motivation behind the above EEG encoder design arises from the inherently under-determined nature of the denoising task. The denoiser tends to exploit any relevant knowledge or informative cues to infer and recover the original data distribution as accurately as possible. This incentivizes the encoder to distill salient commonalities between the source and target EEG signals into a compact representation. We constrain the encoded EEG representation to a low-dimensional latent space and guide the denoiser through feature modulation. This strategy encourages the encoder to capture high-level semantic

<sup>1</sup>Here superscript is used; subscript is reserved for diffusion formation in subsequent sections.

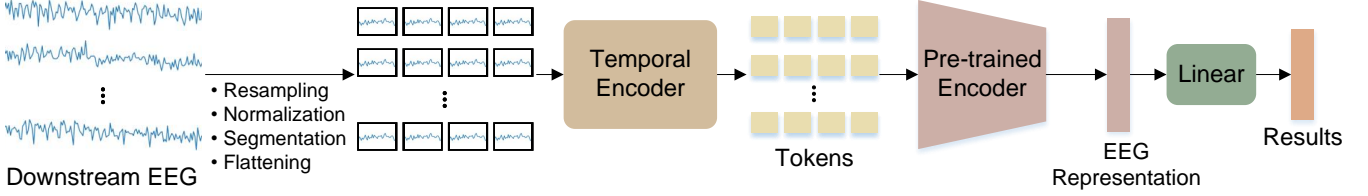


Fig. 2: The pre-trained encoder is connected to a linear prediction head to perform downstream tasks.

information in the EEG signals, while leaving the reconstruction of local details to the denoiser. Rather than reconstruction from scratch as most conventional denoisers do [34], [35], our strategy enables the encoder to learn a representation that supports latent space denoising. This alleviates the burden of compressing all signal information into the representation, allowing it to prioritize the most distinctive and informative features of the EEG. Such a representation is particularly valuable for adapting to a wide range of downstream EEG tasks.

Our EEG encoder is based on the Vision Transformer (ViT) architecture [36] that operates on the sequences of tokens. We segment each EEG channel into tokens and then flatten the tokens to form consistent biosignal sequences. We retain many of ViT's best practices, enabling the EEG encoder to be a Transformer architecture that can process input EEG signals with various formats (different sampling rates, number of channels, and time lengths). The input of the encoder is the source EEG signal  $x'$ , which consists of the original samples and the EEG channel augmentations. EEG augmentations are a set of transformations that preserve the semantic information in the EEG channels without altering the interpretation of the EEG data. Here, we employ two augmentations (zero-masking and amplitude scaling) which were shown in prior work [1] to be the most effective for extracting useful features.

Specifically, we use a  $\omega$ -length window without overlap to segment each EEG channel sample into patches ( $x' = \{x'_{j,k} \in \mathbb{R}^\omega | j = 1, 2, \dots, C, k = 1, 2, \dots, \lfloor \frac{t^s}{\omega} \rfloor\}$ ). The total number of patches for  $x'$  is  $|x'| = C \lfloor \frac{t^s}{\omega} \rfloor$ . Then a temporal encoder (i.e., a temporal convolution block) is used to encode each EEG patch into a patch embedding  $e' = \{e'_{j,k} \in \mathbb{R}^d | j = 1, 2, \dots, C, k = 1, 2, \dots, \lfloor \frac{t^s}{\omega} \rfloor\}$ , where  $d$  is the dimension of the embeddings. The learnable positional embeddings are added to all input patch embeddings. Finally, the sequence of embeddings is fed directly into the Transformer network. We use average pooling on the output embeddings to obtain the EEG representation, which is then combined with the noise timestep representation to guide the denoising of the diffusion model. In addition, we perform downstream EEG tasks by using task-specific prediction heads on the EEG representation. As shown in Fig. 2, we train a linear predictor as the prediction head based on the pre-trained encoder in fine-tuning and then analyze the model's performance on the downstream tasks, in which we employ task-specific loss functions for different downstream objectives. The implementation details can be found in the

subsection IV-B.

### C. EEG Data Generation by Diffusion Model

As aforementioned, due to the inherently low SNR of original EEG signals, accurate reconstruction of them directly in the denoising process is challenging. To address this, we first enhance the SNR of the raw EEG signals using PCA. Similar to the LDMs [14], we find a perceptually equivalent yet computationally more suitable space in which the diffusion model is trained for generating high-SNR EEG signals. In addition, we use the high-quality representation from the EEG encoder to guide the diffusion process. After denoising in the latent space, we apply inverse PCA to project the latent EEG representations back to the original signal space, thereby reconstructing the final EEG signals.

1) *Diffusion Formulation*: The input to our proposed latent diffusion model, which is conditioned on channel augmentation, is the latent representation  $z = Px$  obtained through PCA pre-processing. Here, we use the  $\omega$ -length window to segment each  $x$  before applying PCA to obtain the corresponding latent representation. The PCA basis vectors are computed via eigen-decomposition without the need for gradient-based training. Our diffusion model operates within this latent space. The noisy input  $z_t$  at a given timestep is transformed into patches, which are then linearly embedded into a sequence of tokens with dimension  $d$  (implemented by the patchify layer). Here, we apply a sine-cosine version of the positional embeddings to all input tokens. Then, the input tokens are processed by several DiT blocks. By applying the reparameterization trick, we can do the sampling as follows:

$$z_t = \sqrt{\bar{\alpha}_t} z_0 + \sqrt{1 - \bar{\alpha}_t} \epsilon_t, \quad (1)$$

where  $\epsilon_t \sim \mathcal{N}(0, \mathbf{I})$ . The diffusion model is trained to learn the reverse denoising process:

$$p_\theta(z_{t-1}|z_t) = \mathcal{N}(\mu_\theta(z_t), \Sigma_\theta(z_t)), \quad (2)$$

where the network is used to predict the statistics of  $p_\theta$ . By reparameterizing  $\mu_\theta$  as a noise prediction network (i.e., denoiser)  $\epsilon_\theta$ , the model can be trained using the mean squared error between the predicted noise  $\epsilon_\theta(z_t)$  and the ground truth sampled Gaussian noise  $\epsilon_t$ :

$$\mathcal{L}_{simple}(\theta) = \|\epsilon_\theta(z_t) - \epsilon_t\|_2^2. \quad (3)$$

To train the diffusion model with a learned reverse process covariance  $\Sigma_\theta$ , we follow the approach of Nichol et al. [37]:

train  $\epsilon_\theta$  with  $\mathcal{L}_{simple}$  and train  $\Sigma_\theta$  with  $\mathcal{L}_{vlb}$ . After the final DiT block, we use a standard linear decoder to decode the token sequence into an output noise prediction and an output diagonal covariance prediction. Both outputs have the same data shape as the input. Once  $p_\theta$  is trained, new latent representations can be sampled by initializing  $z_{t_{max}} \sim \mathcal{N}(0, \mathbf{I})$  and sampling  $z_{t-1} \sim p_\theta(z_{t-1}|z_t)$  via the reparameterization trick. Finally, we obtain the denoised latent representation  $\tilde{z}$ , which is then projected back to the original signal space using inverse PCA to reconstruct the original EEG signals:

$$\tilde{x} = P^{-1}\tilde{z} = P^T\tilde{z}. \quad (4)$$

2) *Conditional Guidance*: We incorporate the encoded EEG representation as conditional input for the diffusion model. It guides the generative process and is further leveraged for downstream tasks. To this end, we broadly consider EEG signals in this context as any collection of EEG recordings that exhibit meaningful interrelationships (e.g., semantic correlations), particularly those derived through various augmentations of source EEG signals — an approach well-established in contrastive learning frameworks (Chen et al., 2020). Specifically, each augmented EEG signal is encoded using a shared EEG encoder, and the resulting EEG representations  $e^{1:m}$  are aggregated into a single vector  $e$  by taking their mean, enabling the model to incorporate richer conditional information. When the conditional input is  $e$ , the reverse process of the diffusion model is  $p_\theta(z_{t-1}|z_t, e)$ , where both  $\epsilon_\theta$  and  $\Sigma_\theta$  are conditioned on  $e$ . Under this setting, classifier-free guidance [38] can be applied to encourage the sampling process to find  $z$  such that  $\log p(e|z)$  is maximized. According to Bayes’ rule,  $p(e|z) \propto p(z|e)/p(z)$ , and thus  $\nabla_z \log p(e|z) \propto \nabla_z \log p(z|e) - \nabla_z \log p(z)$ . By interpreting the output of the diffusion model as a score function, the sampling process can be guided by:

$$\begin{aligned} \tilde{\epsilon}_\theta(z_t, e) &\propto \epsilon_\theta(z_t, \emptyset) + s \cdot (\epsilon_\theta(z_t, e) - \epsilon_\theta(z_t, \emptyset)), \\ \tilde{\epsilon}_\theta(z_t, e) &= \epsilon_\theta(z_t, \emptyset) + s \cdot (\nabla_z \log p(z|e)), \end{aligned} \quad (5)$$

where  $s > 1$  denotes the scale of the guidance. The diffusion model with  $e = \emptyset$  is trained by randomly dropping  $e$  during training and replacing it with a learned null embedding  $\emptyset$ . The classifier-free guidance sampling method can significantly improve the quality of generated samples by effectively utilizing the conditional information we introduced.

3) *Conditional Input Setup*: The treatment of conditional inputs and the initialization process significantly influence the generation quality in diffusion models. We adopt the adaLN-Zero block from DiT, which has shown superior performance, to handle the conditional inputs (the EEG representations  $e$  and the noise timestep  $t$ ). Specifically, we regress the scale and shift parameters  $\gamma$  and  $\beta$  in the Transformer blocks based on the sum of the  $e$  and  $t$ . Additionally, we regress the dimension-wise scaling parameters  $\alpha$ , which are applied just before each residual connection in the DiT blocks. The MLP for all  $\alpha$  is initialized to output the zero vector, which effectively initializes the entire DiT block as an identity function. In addition to layer normalization, we incorporate conditional embeddings into residual connections, which enhance the vanilla adaLN and improve the quality of the generated EEG signals.

## IV. EXPERIMENT

### A. Datasets

*Pre-training datasets.* We utilize the Temple University Hospital EEG Corpus (**TUEG**) [39] to pre-train the proposed EEGDM. TUEG is a very large publicly available clinical EEG dataset containing clinical-grade recordings collected in real-world hospital environments. It has over 40 different channel configurations and varying temporal durations of recordings. The majority of the recordings are acquired at a sampling rate of 256 Hz. TUEG exhibits substantial heterogeneity in patient demographics, channel configurations, and recording equipment, making it particularly suitable for pre-training our model.

*Datasets of downstream specific tasks.* (1) **TUEV** (event type classification) [40]: An EEG dataset containing six event categories: spike and sharp wave (SPSW), generalized periodic epileptiform discharges (GPED), periodic lateralized epileptiform discharges (PLED), eye movement (EYEM), artifact (ARTF), and background (BCKG). The EEG signals are recorded at 23 channels and 256 Hz sampling rate. (2) **TUAB** (abnormal detection) [41]: A corpus of EEG recordings annotated as either normal or abnormal. Similar to TUEV, the EEG signals of TUAB are recorded at 23 channels and 256 Hz sampling rate. (3) **SHU-MI** (motor imagery classification) [42]: An EEG motor imagery dataset designed for decoding imagined movements. It features 32 EEG channels sampled at 250 Hz, including two types of motor imagery tasks: left hand and right hand. (4) **CL-Drive** (cognitive load assessment) [43]: It is a multimodal dataset designed for cognitive load assessment, which includes EEG signals. The EEG data are recorded using four channels at a sampling frequency of 256 Hz. This study explores the ternary classification of cognitive load into high, medium, and low levels. (5) **Seed-VII** (emotion recognition) [44]: It is a large-scale multimodal emotion dataset. Seed-VII includes 62-channel EEG and eye-movement data from 20 healthy subjects across seven emotion categories (disgust, fear, sad, neutral, happy, anger, surprise). The preprocessed EEG signals were downsampled to 200 Hz. (6) **DMER** (emotion distribution prediction) [45]: It is a multimodal emotion recognition corpus that includes EEG signals along with other modalities (GSR, PPG, and frontal facial videos). In each trial, participants watched video clips and subsequently completed a self-assessment using a ten-item version of the Positive Affect and Negative Affect Schedule (PANAS) [46], reporting the intensity of ten emotional adjectives. Each emotion rating ranges from 1 (not at all) to 5 (extremely), and the resulting scores are transformed into a 10-dimensional emotion distribution. The EEG recordings comprise 18 channels sampled at 300 Hz.

It is worth noting that we primarily select downstream datasets from the past five years, a strategic shift from the benchmarks used in works like CBraMod [8] or EEGPT [6]. This decision stems from the need to evaluate the model against the fidelity and complexity of modern neuroscience standards. Older datasets often lack the high spatial density and signal quality required to stress-test a foundation model, whereas recent paradigms — ranging from naturalistic stimuli

to multimodal retrieval — better assess the capacity for generalizable, high-level cognitive decoding. However, to ensure fair comparison with established baselines, we make exceptions for the TUAB and TUEV datasets. Despite falling outside the five-year window, these two widely adopted benchmarks are retained as standardized anchors, allowing us to validate our model’s performance on classical clinical tasks alongside its capabilities on modern, complex scenarios.

### B. Experimental Setup

For the pre-training dataset TUEG, following prior work [8], we select 19 common EEG channels. All EEG signals are resampled to 200 Hz and segmented into non-overlapping 30-second samples (19 channels  $\times$  6,000 time points). Each EEG patch is set to a temporal length of 1 second, resulting in 570 patches per sample. For all downstream datasets, we maintain consistency with our pre-training data by resampling EEG signals to 200 Hz and setting each EEG patch duration to 1 second.

For the downstream datasets TUEV and TUAB, consistent with previous studies [6]–[8], we utilize 16 common bipolar montage channels from the international 10-20 system, with sample durations of 5 seconds and 10 seconds, respectively. We adopt the train-test splits provided by these datasets. For the CL-Drive dataset, we use the channel configuration and sample duration (10 seconds) provided by the dataset and apply 10-fold subject-wise cross-validation. For the SHU-MI, DMER, and SEED-VII datasets, we use the channel configurations provided by each dataset and segment the signals into 4-second samples. We employ a subject-independent split strategy for these datasets. We fine-tune EEGPT [6], LaBraM-Base [7] (the only variant with available pre-trained weights), and CBraMod [8] based on their publicly available code and pre-trained weights, except when their experimental results are already reported in the original papers.

For the EEG generator (diffusion module) and encoder, we adopt the DiT and ViT architectures, respectively. Following common practices in generative modeling literature, we maintain an exponential moving average (EMA) of model weights with a decay rate of 0.9999 during pre-training. The specific hyperparameters for pre-training are detailed in Table I.

We evaluate the representation learning capabilities of EEGDM through fine-tuning on downstream tasks. Specifically, we predict corresponding labels using a linear predictor based on the outputs of the EEG encoder. Following the common evaluation protocols, we present results under the fine-tuning setting, where the predictor is jointly trained with the EEG encoder (i.e., the pre-trained encoder is not frozen). We employ cross-entropy loss for downstream classification tasks and KL divergence loss for downstream distribution prediction tasks. The hyperparameters for fine-tuning EEGDM on downstream tasks are provided in Table II. We conduct a series of quantitative and qualitative experiments to evaluate the proposed model, demonstrating its strong representation capabilities across diverse downstream datasets.

TABLE I: Hyperparameters for EEGDM pre-training.

	Hyperparameter	Value
Optimization	Batch size	32
	Peak learning rate	5e-4
	Minimal learning rate	5e-5
	Learning rate scheduler	OneCycleLR
	Weight decay	0.05
	EMA decay rate	0.9999
	Gradient clipping norm	1
	Optimizer	AdamW
	$\beta_1$	0.9
	$\beta_2$	0.999
EEG Generator	Layers N	8
	Hidden size	512
	Heads	8
	Normalization type	LayerNorm
EEG Encoder	Layers	8
	Hidden size	512
	MLP size	2048
	Heads	8
Sampling	Classifier-free guidance	9
	Diffusion training steps	1000

TABLE II: Hyperparameters for downstream fine-tuning. (\*) Depends on the dataset.

	Hyperparameter	Value
Optimization	Batch size	64
	Peak learning rate	5e-4
	Minimal learning rate	5e-5
	Learning rate scheduler	OneCycleLR
	Optimizer	AdamW
	$\beta_1$	0.9
	$\beta_2$	0.999
	Weight decay	0.05
	Total epochs*	30, 150
Warmup Epochs*	Warmup Epochs*	6, 30

### C. Results and Analysis

In this section, we show that EEGDM achieves competitive performance across diverse downstream tasks, demonstrating the effectiveness of diffusion-based representation learning for EEG analysis. All experiments are conducted with multiple random seeds, and we report the mean and standard deviation of evaluation metrics. The reported model size corresponds to the downstream networks used for fine-tuning, as the generative module is not involved in downstream tasks. Results are compared against baselines, as shown in Tables III, IV, V and VI. Compared to other approaches, EEGDM consistently maintains either the best or second-best performance in key metrics (balanced accuracy or KL divergence).

On the TUEV dataset, EEGDM achieves a balanced accuracy of 68.19%, outperforming both the previous state-of-the-art method CBraMod (66.71%) and other baselines. This superiority highlights the exceptional discriminative power of the representations learned by the diffusion model for classifying different event types in EEG signals.

Table IV shows that EEGDM achieves a balanced accuracy of 81.80% and an AUC-PR of 90.85% on the TUAB dataset. Securing the second-best performance on those metrics, EEGDM overall demonstrates comparable performance with a competitive margin. The consistent performance across both balanced accuracy and AUC-PR metrics suggests that EEGDM learns robust representations that generalize well for binary

TABLE III: Performance comparison on TUEV. The best metric is highlighted in bold, and the second-best metric is underlined.

Methods	Params	Balanced Accuracy $\uparrow$	Weighted F1 $\uparrow$	Cohen’s Kappa $\uparrow$
ST-Transformer [47]	3.5M	0.3984 $\pm$ 0.0228	0.6823 $\pm$ 0.0190	0.3765 $\pm$ 0.0306
ContraWR [48]	1.6M	0.4384 $\pm$ 0.0349	0.6893 $\pm$ 0.0136	0.3912 $\pm$ 0.0237
CNN-Transformer [49]	3.2M	0.4087 $\pm$ 0.0161	0.6854 $\pm$ 0.0293	0.3815 $\pm$ 0.0134
FFCL [50]	2.4M	0.3979 $\pm$ 0.0104	0.6783 $\pm$ 0.0120	0.3732 $\pm$ 0.0188
SPaRCNet [51]	0.79M	0.4161 $\pm$ 0.0262	0.7024 $\pm$ 0.0104	0.4233 $\pm$ 0.0181
BIOT [52]	3.2M	0.5281 $\pm$ 0.0225	0.7492 $\pm$ 0.0082	0.5273 $\pm$ 0.0249
EEGPT [6]	25M	0.6232 $\pm$ 0.0114	0.8187 $\pm$ 0.0063	0.6351 $\pm$ 0.0134
LaBraM-Base [7]	5.8M	0.6409 $\pm$ 0.0065	0.8312 $\pm$ 0.0052	0.6637 $\pm$ 0.0093
CBraMod [8]	4.0M	<u>0.6671<math>\pm</math>0.0107</u>	<b>0.8342<math>\pm</math>0.0064</b>	<b>0.6772<math>\pm</math>0.0096</b>
EEGDM	25M	<b>0.6819<math>\pm</math>0.0084</b>	0.7362 $\pm$ 0.0416	0.5097 $\pm$ 0.0676

TABLE IV: Performance comparison on TUAB. The best metric is highlighted in bold, and the second-best metric is underlined.

Methods	Params	Balanced Accuracy $\uparrow$	AUROC $\uparrow$	AUC-PR $\uparrow$
ST-Transformer [47]	3.5M	0.7966 $\pm$ 0.0023	0.8707 $\pm$ 0.0019	0.8521 $\pm$ 0.0026
ContraWR [48]	1.6M	0.7746 $\pm$ 0.0041	0.8456 $\pm$ 0.0074	0.8421 $\pm$ 0.0104
CNN-Transformer [49]	3.2M	0.7777 $\pm$ 0.0022	0.8461 $\pm$ 0.0013	0.8433 $\pm$ 0.0039
FFCL [50]	2.4M	0.7848 $\pm$ 0.0038	0.8569 $\pm$ 0.0051	0.8448 $\pm$ 0.0065
SPaRCNet [51]	0.79M	0.7896 $\pm$ 0.0018	0.8676 $\pm$ 0.0012	0.8414 $\pm$ 0.0018
BIOT [52]	3.2M	0.7959 $\pm$ 0.0057	0.8815 $\pm$ 0.0043	0.8792 $\pm$ 0.0023
EEGPT [6]	25M	0.7983 $\pm$ 0.0030	0.8718 $\pm$ 0.0050	/
LaBraM-Base [7]	5.8M	0.8140 $\pm$ 0.0019	0.9022 $\pm$ 0.0009	0.8965 $\pm$ 0.0016
CBraMod [8]	4.0M	<b>0.8289<math>\pm</math>0.0022</b>	<u>0.9227<math>\pm</math>0.0011</u>	<b>0.9258<math>\pm</math>0.0008</b>
EEGDM	25M	<u>0.8180<math>\pm</math>0.0013</u>	0.8922 $\pm$ 0.0009	<u>0.9085<math>\pm</math>0.0002</u>

TABLE V: Performance comparison on DMER. The best metric is highlighted in bold, and the second-best metric is underlined.

Methods	Chebyshev $\downarrow$	Clark $\downarrow$	Canberra $\downarrow$	KL $\downarrow$	Cosine $\uparrow$	Intersection $\uparrow$
EEGPT [6]	0.1016 $\pm$ 0.0020	0.3009 $\pm$ 0.0055	<u>1.7264<math>\pm</math>0.0204</u>	0.1055 $\pm$ 0.0045	0.9005 $\pm$ 0.0042	0.8172 $\pm$ 0.0026
LaBraM-Base [7]	<u>0.0925<math>\pm</math>0.0064</u>	<b>0.2924<math>\pm</math>0.0048</b>	1.7476 $\pm$ 0.0287	<u>0.0995<math>\pm</math>0.0038</u>	0.9094 $\pm$ 0.0037	0.8198 $\pm$ 0.0034
CBraMod [8]	0.0945 $\pm$ 0.0052	0.3024 $\pm$ 0.0286	1.8320 $\pm$ 0.1984	<u>0.1077<math>\pm</math>0.0148</u>	0.9026 $\pm$ 0.0116	0.8104 $\pm$ 0.0184
EEGDM	<b>0.0836<math>\pm</math>0.078</b>	<u>0.2984<math>\pm</math>0.0053</u>	<b>1.6112<math>\pm</math>0.0108</b>	<b>0.0978<math>\pm</math>0.0063</b>	<b>0.9176<math>\pm</math>0.0083</b>	<b>0.8258<math>\pm</math>0.0047</b>

abnormal detection tasks, maintaining high discriminative power even in challenging clinical scenarios.

Table V presents the results for the DMER dataset, which uses distributional metrics. EEGDM achieves best performance across various divergence and similarity metrics, with the exception of the Clark metric, where it ranks second. The overall high performance on DMER, a task requiring the prediction of a continuous emotion distribution rather than a discrete class, strongly suggests that the diffusion-based pre-training learns rich and fine-grained features that preserve the complex, subtle, and continuous emotional states embedded in the EEG signals.

Table VI further validates the generalizability and robustness of EEGDM across diverse BCI tasks. Specifically, on the SHU-MI dataset, EEGDM ranks second in terms of balanced accuracy (63.24%) and AUC-PR (70.70%), while achieving the best performance in AUROC (69.96%), demonstrating competitive performance compared with CBraMod. For the CL-Drive dataset, EEGDM shows the best balanced accuracy and the best Cohen’s Kappa, demonstrating superior cognitive load feature extraction capabilities. On the Seed-VII dataset, EEGDM continues its strong performance with the best performance in balanced accuracy and ranks second in weighted F1 and Cohen’s Kappa, further validating its effectiveness in emotion-related tasks.

These comprehensive results across diverse datasets validate the effectiveness of using EEG signal generation as a self-supervised pre-training objective, demonstrating that the combination of encoder and diffusion denoiser, enhanced by PCA and channel augmentation, successfully learns high-quality EEG representations for improved downstream task performance.

#### D. Ablation Study

We conduct ablation studies to analyze the contributions of PCA and channel augmentation components, respectively, by setting up four variant versions as shown in Table VII, in which the average balanced accuracy on three random seeds is reported. Variant D consistently achieves the best performance across all settings, demonstrating that PCA and EEG augmentation are important for our model. However, we find that using PCA or EEG augmentation alone is either detrimental to or has minimal impact on our model’s performance. This may be attributed to the fact that PCA reduces the dimensionality of the source signal, making the model more sensitive to the diversity of conditional information, while data augmentation provides sufficient diversity to support learning in this reduced-dimensional space. Consequently, the PCA and EEG augmentation operations achieve complementary effects in terms of generalization performance and accuracy. Furthermore, for TUAB, we randomly selected 10% of the

TABLE VI: The results of different methods on various datasets. The best metric is highlighted in bold, and the second-best metric is underlined.

Datasets	Methods	Balanced Accuracy $\uparrow$	Weighted F1 / AUROC $\uparrow$	Cohen's Kappa / AUC-PR $\uparrow$
SHU-MI	EEGPT [6]	0.5565 $\pm$ 0.0345	0.5908 $\pm$ 0.0502	0.5996 $\pm$ 0.0491
	LaBraM-Base [7]	0.6166 $\pm$ 0.0192	0.6604 $\pm$ 0.0091	0.6761 $\pm$ 0.0083
	CBraMod [8]	<b>0.6370<math>\pm</math>0.0151</b>	0.6988 $\pm$ 0.0068	<b>0.7139<math>\pm</math>0.0088</b>
CL-Drive	EEGDM	<u>0.6324<math>\pm</math>0.0052</u>	<b>0.6996<math>\pm</math>0.0035</b>	<u>0.7070<math>\pm</math>0.0061</u>
	EEGPT [6]	0.4674 $\pm$ 0.0562	<b>0.5038<math>\pm</math>0.0640</b>	0.1641 $\pm$ 0.0894
	LaBraM-Base [7]	0.4096 $\pm$ 0.0942	0.4438 $\pm$ 0.0972	0.0745 $\pm$ 0.1087
Seed-VII	CBraMod [8]	<u>0.5346<math>\pm</math>0.0856</u>	0.4896 $\pm$ 0.1237	0.2322 $\pm$ 0.1014
	EEGDM	<b>0.5357<math>\pm</math>0.0557</b>	<u>0.5019<math>\pm</math>0.0725</u>	<b>0.2944<math>\pm</math>0.0841</b>
	EEGPT [6]	0.2125 $\pm$ 0.0112	0.1989 $\pm$ 0.0264	0.0849 $\pm$ 0.0159
Seed-VII	LaBraM-Base [7]	<u>0.2281<math>\pm</math>0.0077</u>	<b>0.2198<math>\pm</math>0.0113</b>	<b>0.1003<math>\pm</math>0.0090</b>
	CBraMod [8]	0.2027 $\pm$ 0.0045	0.1824 $\pm$ 0.0034	0.0731 $\pm$ 0.0041
	EEGDM	<b>0.2300<math>\pm</math>0.0021</b>	<u>0.2115<math>\pm</math>0.0087</u>	0.0943 $\pm$ 0.0395

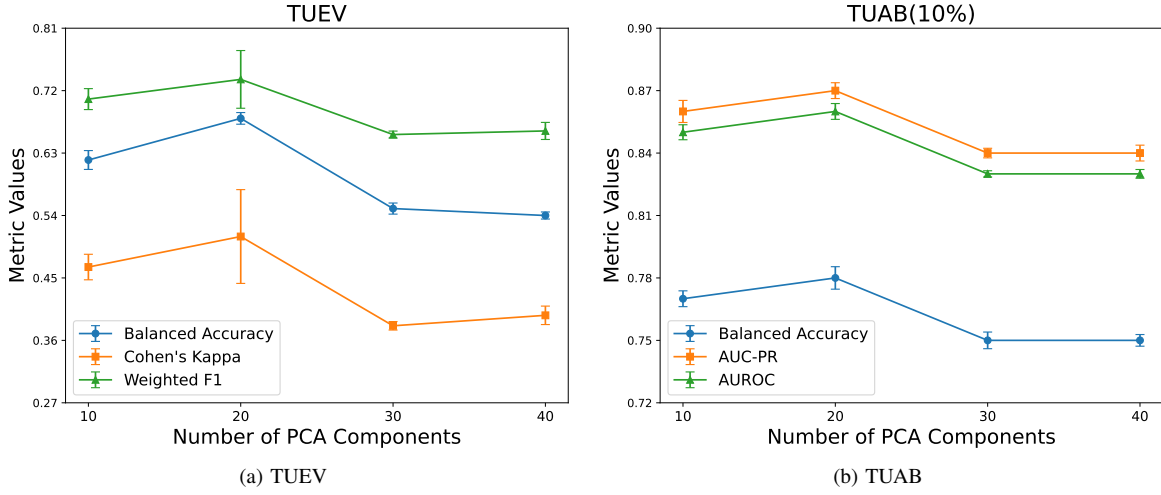


Fig. 3: Performance comparison with different numbers of PCA components on TUEV and TUAB datasets.

TABLE VII: The results of the ablation studies for PCA and EEG augmentation, using the metric of average balanced accuracy.

Variants	PCA	EEG Augmentation	TUEV	TUAB (10%)
A	$\times$	$\times$	0.6038 $\pm$ 0.0053	0.7570 $\pm$ 0.0043
B	$\checkmark$	$\times$	0.5759 $\pm$ 0.0060	0.7556 $\pm$ 0.0027
C	$\times$	$\checkmark$	0.5994 $\pm$ 0.0144	0.7587 $\pm$ 0.0053
D	$\checkmark$	$\checkmark$	0.6819 $\pm$ 0.0084	0.7815 $\pm$ 0.0054

training set for fine-tuning and tested it on the entire test set (see the last column in Table VII); we also use this setting in Fig. 3. The results show that the advantages of incorporating PCA and EEG augmentation remain evident even when small-scale datasets are used for fine-tuning.

We also investigate the impact of the number of PCA components on downstream task performance. Fig. 3 presents results on TUEV and TUAB with varying numbers of PCA components, which reveal a nonlinear relationship between the number of PCA components and downstream task performance. In particular, insufficient number of components may result in large information loss, whereas an excessive number

introduces noise contamination, both of which degrade model performance. To balance these trade-offs, we empirically select an intermediate value of 20 components, which yields optimal performance in our experiments.

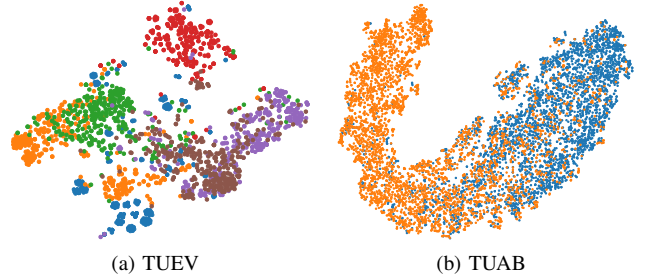


Fig. 4: The t-SNE visualizations. Clear inter-class separation and intra-class compactness indicate that the learned representations are discriminative.

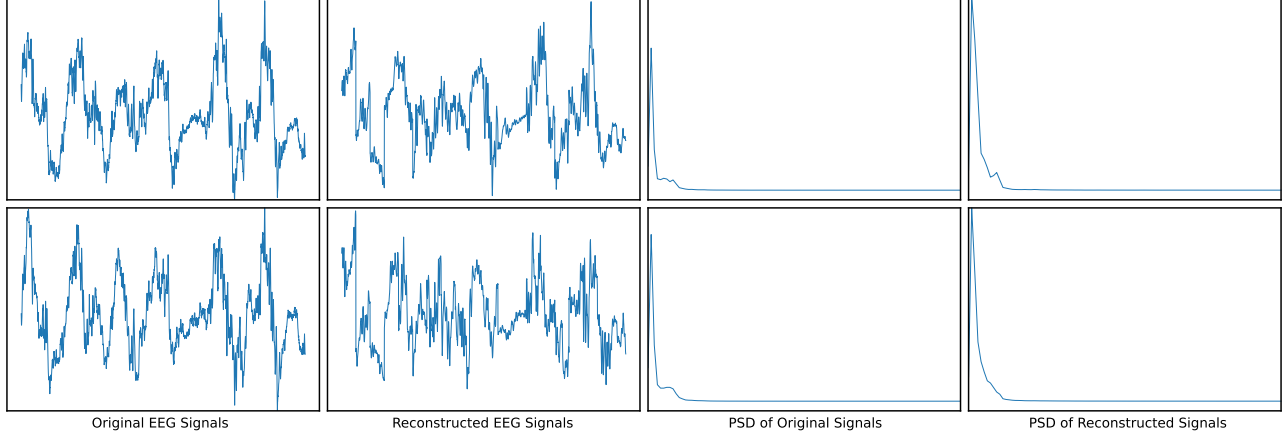


Fig. 5: Visualization of reconstructed EEG signals and their PSD.

### E. Visualization

To evaluate the quality of learned representations, we visualize the EEG data embeddings using t-SNE [53] as presented in Fig. 4. We randomly sample EEG signals from the test sets of two downstream tasks in a class-balanced manner and extract their representations using our pre-trained encoder. The t-SNE visualizations exhibit well-separated clusters across all datasets, indicating that our EEGDM learns discriminative representations capable of capturing task-relevant patterns. This clear clustering structure further demonstrates the EEGDM’s ability to learn generic yet informative EEG representations that can be successfully adapted to diverse downstream tasks.

Beyond representation learning, EEGDM also achieves high-quality EEG signal reconstruction, as evidenced by visualizations of reconstructed signals and their power spectral density (PSD) analyses. As shown in Fig. 5, the reconstructed EEG signals on the pre-training dataset, as well as their frequency-domain representations, closely match the ground truth. While minor discrepancies remain at the fine-grained level, the global temporal structure and frequency characteristics are well preserved. These results indicate that the proposed model can generate realistic EEG signals and effectively capture high-level semantic information from EEG data.

In summary, our experimental results highlight three key advantages of EEGDM: (1) *High-quality EEG reconstruction*, as validated by signal reconstruction visualization; (2) *Effective representation learning*, as demonstrated by distinct class separation in t-SNE visualization; and (3) *Competitive performance* across diverse downstream tasks, as evidenced by consistent performance improvements across tasks.

## V. CONCLUSION

We present EEGDM, a novel latent diffusion framework for EEG representation learning, through explicit conditioning on EEG channel augmentation. Our EEGDM takes the generative task as the self-supervised EEG representation learning objective. By (1) integrating a denoiser with the EEG encoder and (2) making use of PCA-based projection and EEG channel augmentation, EEGDM can perform the generation task in the

latent space using rich conditional information while learning powerful EEG semantic representations that can be applied to diverse downstream tasks. Comprehensive experimental results demonstrate the model’s effectiveness across multiple downstream tasks.

## REFERENCES

- [1] M. N. Mohsenvand, M. R. Izadi, P. Maes, and P. Maes, “Contrastive representation learning for electroencephalogram classification,” in *Machine Learning for Health*, 2020, pp. 238–253.
- [2] T. O. Zander and C. Kothe, “Towards passive brain–computer interfaces: applying brain–computer interface technology to human–machine systems in general,” *Journal of neural engineering*, vol. 8, no. 2, p. 025005, 2011.
- [3] L.-M. Zhao, X. Yan, and B.-L. Lu, “Plug-and-play domain adaptation for cross-subject eeg-based emotion recognition,” in *Proceedings of the AAAI conference on artificial intelligence*, vol. 35, no. 1, 2021, pp. 863–870.
- [4] R. Zheng, J. Li, Y. Wang, T. Luo, and Y. Yu, “Scatterformer: locally-invariant scattering transformer for patient-independent multispectral detection of epileptiform discharges,” in *Proceedings of the AAAI conference on artificial intelligence*, vol. 37, no. 1, 2023, pp. 148–158.
- [5] Z. Chen, Y. Matsubara, Y. Sakurai, and J. Sun, “Long-term eeg partitioning for seizure onset detection,” in *Proceedings of the AAAI conference on artificial intelligence*, vol. 39, no. 13, 2025, pp. 14 221–14 229.
- [6] G. Wang, W. Liu, Y. He, C. Xu, L. Ma, and H. Li, “Eegpt: Pretrained transformer for universal and reliable representation of eeg signals,” in *The Thirty-eighth Annual Conference on Neural Information Processing Systems*, 2024.
- [7] W.-B. Jiang, L.-M. Zhao, and B.-L. Lu, “Large brain model for learning generic representations with tremendous eeg data in bci,” in *International conference on learning representations*, 2024.
- [8] J. Wang, S. Zhao, Z. Luo, Y. Zhou, H. Jiang, S. Li, T. Li, and G. Pan, “Cbramod: A criss-cross brain foundation model for eeg decoding,” *International conference on learning representations*, 2025.
- [9] J. Ho, A. Jain, and P. Abbeel, “Denoising diffusion probabilistic models,” *Advances in neural information processing systems*, vol. 33, pp. 6840–6851, 2020.
- [10] P. Dhariwal and A. Nichol, “Diffusion models beat gans on image synthesis,” *Advances in neural information processing systems*, vol. 34, pp. 8780–8794, 2021.
- [11] A. Gramfort, D. Strohmeier, J. Haueisen, M. S. Hämäläinen, and M. Kowalski, “Time-frequency mixed-norm estimates: Sparse m/eeg imaging with non-stationary source activations,” *NeuroImage*, vol. 70, pp. 410–422, 2013.
- [12] S. Cole and B. Voytek, “Cycle-by-cycle analysis of neural oscillations,” *Journal of neurophysiology*, vol. 122, no. 2, pp. 849–861, 2019.
- [13] S. Sanei and J. A. Chambers, *EEG signal processing*. John Wiley & Sons, 2013.

[14] R. Rombach, A. Blattmann, D. Lorenz, P. Esser, and B. Ommer, "High-resolution image synthesis with latent diffusion models," in *Proceedings of the IEEE/CVF conference on computer vision and pattern recognition*, 2022, pp. 10684–10695.

[15] W. Peebles and S. Xie, "Scalable diffusion models with transformers," in *Proceedings of the IEEE/CVF international conference on computer vision*, 2023, pp. 4195–4205.

[16] J. D. M.-W. C. Kenton and L. K. Toutanova, "Bert: Pre-training of deep bidirectional transformers for language understanding," in *Proceedings of naacl-HLT*, vol. 1, 2019, p. 2.

[17] K. He, X. Chen, S. Xie, Y. Li, P. Dollár, and R. Girshick, "Masked autoencoders are scalable vision learners," in *Proceedings of the IEEE/CVF conference on computer vision and pattern recognition*, 2022, pp. 16 000–16 009.

[18] W.-B. Jiang, Y. Wang, B.-L. Lu, and D. Li, "Neurolm: A universal multi-task foundation model for bridging the gap between language and eeg signals," in *International conference on learning representations*, 2025.

[19] H. Banville, O. Chehab, A. Hyvärinen, D.-A. Engemann, and A. Gramfort, "Uncovering the structure of clinical eeg signals with self-supervised learning," *Journal of Neural Engineering*, vol. 18, no. 4, p. 046020, 2021.

[20] T. Chen, S. Kornblith, M. Norouzi, and G. Hinton, "A simple framework for contrastive learning of visual representations," in *International conference on machine learning*, 2020, pp. 1597–1607.

[21] N. Mohammadi Foumani, G. Mackellar, S. Ghane, S. Irtza, N. Nguyen, and M. Salehi, "Eeg2rep: enhancing self-supervised eeg representation through informative masked inputs," in *Proceedings of the 30th ACM SIGKDD Conference on Knowledge Discovery and Data Mining*, 2024, pp. 5544–5555.

[22] H.-Y. S. Chien, H. Goh, C. M. Sandino, and J. Y. Cheng, "Maeeg: Masked auto-encoder for eeg representation learning," *arXiv preprint arXiv:2211.02625*, 2022.

[23] D. Kostas, S. Aroca-Ouellette, F. Rudzicz, and F. Rudzicz, "Bendr: Using transformers and a contrastive self-supervised learning task to learn from massive amounts of eeg data," *Frontiers in Human Neuroscience*, vol. 15, p. 653659, 2021.

[24] J. Sohl-Dickstein, E. Weiss, N. Maheswaranathan, and S. Ganguli, "Deep unsupervised learning using nonequilibrium thermodynamics," in *International conference on machine learning*, 2015, pp. 2256–2265.

[25] L. Zhang, A. Rao, and M. Agrawala, "Adding conditional control to text-to-image diffusion models," in *Proceedings of the IEEE/CVF international conference on computer vision*, 2023, pp. 3836–3847.

[26] S. Mittal, K. Abstreiter, S. Bauer, B. Schölkopf, and A. Mehrjou, "Diffusion based representation learning," in *International conference on machine learning*, 2023, pp. 24 963–24 982.

[27] X. Chen, Z. Liu, S. Xie, and K. He, "Deconstructing denoising diffusion models for self-supervised learning," *arXiv preprint arXiv:2401.14404*, 2024.

[28] D. A. Hudson, D. Zoran, M. Malinowski, A. K. Lampinen, A. Jaegle, J. L. McClelland, L. Matthey, F. Hill, and A. Lerchner, "Soda: Bottleneck diffusion models for representation learning," in *Proceedings of the IEEE/CVF conference on computer vision and pattern recognition*, 2024, pp. 23 115–23 127.

[29] X. Huang, C. Li, A. Liu, R. Qian, and X. Chen, "Eegdfus: A conditional diffusion model for fine-grained eeg denoising," *IEEE Journal of Biomedical and Health Informatics*, 2024.

[30] M. Chen, Y. Gui, Y. Su, Y. Zhu, G. Luo, and Y. Yang, "Improving eeg classification through randomly reassembling original and generated data with transformer-based diffusion models," *arXiv*, 2024.

[31] J. Huang, M. Li, and W. Chen, "Sad-ver: A self-supervised, diffusion probabilistic model-based data augmentation framework for visual-stimulus eeg recognition," *Advanced Engineering Informatics*, vol. 65, p. 103298, 2025.

[32] S. Kim, Y.-E. Lee, S.-H. Lee, and S.-W. Lee, "Diff-e: Diffusion-based learning for decoding imagined speech eeg," *arXiv preprint arXiv:2307.14389*, 2023.

[33] S. Kim, S.-H. Lee, Y.-E. Lee, J.-W. Lee, J.-H. Park, P. Kazanzides, and S.-W. Lee, "Brain-driven representation learning based on diffusion model," in *2024 12th International Winter Conference on Brain-Computer Interface (BCI)*, 2024, pp. 1–4.

[34] G. E. Hinton and R. R. Salakhutdinov, "Reducing the dimensionality of data with neural networks," *science*, vol. 313, no. 5786, pp. 504–507, 2006.

[35] I. Higgins, L. Matthey, A. Pal, C. P. Burgess, X. Glorot, M. M. Botvinick, S. Mohamed, and A. Lerchner, "beta-vae: Learning basic visual concepts with a constrained variational framework," in *International conference on learning representations*, 2017.

[36] A. Dosovitskiy, "An image is worth 16x16 words: Transformers for image recognition at scale," in *International conference on learning representations*, 2021.

[37] A. Q. Nichol and P. Dhariwal, "Improved denoising diffusion probabilistic models," in *International conference on machine learning*, 2021, pp. 8162–8171.

[38] J. Ho and T. Salimans, "Classifier-free diffusion guidance," *arXiv preprint arXiv:2207.12598*, 2022.

[39] I. Obeid and J. Picone, "The temple university hospital eeg data corpus," *Frontiers in neuroscience*, vol. 10, p. 196, 2016.

[40] A. Harati, M. Golmohammadi, S. Lopez, I. Obeid, and J. Picone, "Improved eeg event classification using differential energy," in *2015 IEEE Signal Processing in Medicine and Biology Symposium (SPMB)*, 2015, pp. 1–4.

[41] S. Lopez, G. Suarez, D. Jungreis, I. Obeid, and J. Picone, "Automated identification of abnormal adult eegs," in *2015 IEEE signal processing in medicine and biology symposium (SPMB)*, 2015, pp. 1–5.

[42] J. Ma, B. Yang, W. Qiu, Y. Li, S. Gao, and X. Xia, "A large eeg dataset for studying cross-session variability in motor imagery brain-computer interface," *Scientific Data*, vol. 9, no. 1, p. 531, 2022.

[43] P. Angkan, B. Behinaein, Z. Mahmud, A. Bhatti, D. Rodenburg, P. Hungler, and A. Etemad, "Multimodal brain–computer interface for in-vehicle driver cognitive load measurement: Dataset and baselines," *IEEE Transactions on Intelligent Transportation Systems*, vol. 25, no. 6, pp. 5949–5964, 2024.

[44] W.-B. Jiang, X.-H. Liu, W.-L. Zheng, and B.-L. Lu, "Seed-vii: A multimodal dataset of six basic emotions with continuous labels for emotion recognition," *IEEE Transactions on Affective Computing*, 2024.

[45] P. Yang, N. Liu, X. Liu, Y. Shu, W. Ji, Z. Ren, J. Sheng, M. Yu, R. Yi, D. Zhang *et al.*, "A multimodal dataset for mixed emotion recognition," *Scientific Data*, vol. 11, no. 1, p. 847, 2024.

[46] A. Mackinnon, A. F. Jorm, H. Christensen, A. E. Korten, P. A. Jacomb, and B. Rodgers, "A short form of the positive and negative affect schedule: Evaluation of factorial validity and invariance across demographic variables in a community sample," *Personality and Individual differences*, vol. 27, no. 3, pp. 405–416, 1999.

[47] Y. Song, X. Jia, L. Yang, and L. Xie, "Transformer-based spatial-temporal feature learning for eeg decoding," *arXiv preprint arXiv:2106.11170*, 2021.

[48] C. Yang, C. Xiao, M. B. Westover, J. Sun *et al.*, "Self-supervised electroencephalogram representation learning for automatic sleep staging: model development and evaluation study," *JMIR AI*, vol. 2, no. 1, p. e46769, 2023.

[49] W. Y. Peh, Y. Yao, and J. Dauwels, "Transformer convolutional neural networks for automated artifact detection in scalp eeg," in *2022 44th Annual International Conference of the IEEE Engineering in Medicine & Biology Society (EMBC)*, 2022, pp. 3599–3602.

[50] H. Li, M. Ding, R. Zhang, and C. Xiu, "Motor imagery eeg classification algorithm based on cnn-lstm feature fusion network," *Biomedical signal processing and control*, vol. 72, p. 103342, 2022.

[51] J. Jing, W. Ge, S. Hong, M. B. Fernandes, Z. Lin, C. Yang, S. An, A. F. Struck, A. Herlopian, I. Karakis *et al.*, "Development of expert-level classification of seizures and rhythmic and periodic patterns during eeg interpretation," *Neurology*, vol. 100, no. 17, pp. e1750–e1762, 2023.

[52] C. Yang, M. Westover, and J. Sun, "Biot: Biosignal transformer for cross-data learning in the wild," *Advances in Neural Information Processing Systems*, vol. 36, 2024.

[53] L. Van der Maaten and G. Hinton, "Visualizing data using t-sne," *Journal of machine learning research*, vol. 9, no. 11, 2008.